

# DIVERGENCE FREE SYNTHETIC EDDY METHOD FOR EMBEDDED LES INFLOW BOUNDARY CONDITIONS

R. Poletto, A. Revell, T. Craft, N. Jarrin

School of Mechanical Aerospace and Civil Engineering  
University of Manchester, Manchester, UK  
ruggero.poletto@postgrad.manchester.ac.uk

## ABSTRACT

A new inlet treatment for embedded LES is here proposed. The method, based on the SEM proposed by [1], satisfies the divergence free condition of the velocity field, and hence reduces the pressure fluctuations present in the downstream flow close to the inlet with the original SEM. Results compare the new method against the SEM and the VORTEX method, introduced by [2], for a plane channel flow, showing that the proposed scheme produces fairly realistic inlet turbulence, and hence requires a shorter development length compared to the other two schemes.

## INTRODUCTION

One of the challenges in performing Large Eddy Simulations (LES) of turbulent flows is the prescription of a suitable velocity field at flow inlets. In most cases these should, ideally, correspond to a suitably realistic unsteady flow field; yet at the same time one also wants them to be reasonably cheap to generate. These requirements hold both for full LES applications, and for RANS/LES hybrid approaches, where ‘inlet’ conditions for the LES region must be generated from the RANS solution. It is well known that simply imposing random fluctuations on top of a mean velocity field at an inlet will result in a long development length before the flow reaches what might be considered a realistic turbulent state, and so a number of alternative methods have been developed, aimed at providing more realistic representations of inlet turbulence.

Ref [1] developed the Synthetic Eddy Method (SEM) as a quasi-particle based method to generate synthetic turbulence conditions. The method essentially involves the superposition of a (large) number of random eddies, with some control placed on their statistical properties, which are convected through a domain of rectangular cross-section, such as that shown in Fig. 1. The resultant, time-dependent, flowfield from a cross-section of this SEM domain is extracted and imposed as inlet conditions for the LES. Using this approach [1] found that LES of a channel flow at  $Re_\tau = 395$  required a distance of around 10–12 channel half-widths to become fully-developed. Some further improvements were achieved by [3], by specifically tuning the shape functions associated with the eddy representations for a channel flow. Although they did re-

port a decrease in the required development length, the form adopted would appear to be rather specific to the application.

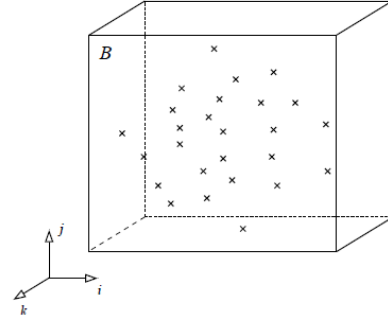


Figure 1. Schematic of the SEM method: the eddies (velocity fluctuations) are generated and convected through an eddy box

One of the perceived weaknesses of the above SEM methods is that the imposed inlet flowfield does not satisfy the divergence-free condition. As a consequence of this the LES tends to introduce significant pressure fluctuations close to the inlet (in order to adapt the velocity field to something that does satisfy continuity), and this adds to the required development length. In the present work, we therefore explore a method of extending the SEM approach in order to produce a suitable inlet velocity field that does satisfy continuity.

## THE DIVERGENCE FREE SEM (DF-SEM)

The DF-SEM is based on the previous version proposed by [1] and [4], with the main difference being the way the velocity fluctuations associated with the eddies are defined. In the SEM these come from the following:

$$\mathbf{u}'(\mathbf{x}) = \frac{1}{\sqrt{N}} \sum_{k=1}^N a_{ij} \epsilon_j^k f_\sigma(\mathbf{x} - \mathbf{x}^k) \quad (1)$$

where  $N$  is the number of eddies introduced into the SEM domain,  $\mathbf{x}^k$  is the location of the centre of the  $k$ th eddy,  $f_\sigma(\mathbf{x})$  is a suitable shape function,  $\varepsilon_j^k$  are random numbers with zero average and  $\langle \varepsilon_j^k \varepsilon_j^k \rangle = 1$  which represent the eddies' intensities, and  $a_{ij}$  are the Lund coefficients as defined by [5]. Although this formulation does allow the desired Reynolds stress field to be prescribed (via the  $a_{ij}$  coefficients), the velocity field will not, in general, also satisfy continuity.

In order to ensure that continuity is satisfied, the DF-SEM applies the SEM approach to the vorticity field and then transforms this back to give a resulting velocity field. Equation (1) is thus applied to the vorticity field, in order to generate fluctuations in it. The curl of the vorticity is then related to the velocity Laplacian by

$$\nabla \times \omega' = \nabla(\nabla \cdot \mathbf{u}') - \nabla^2 \mathbf{u}' \quad (2)$$

where, obviously, the first term on the right hand side of equation (2) is neglected because of the divergence free condition. The solution of this Poisson equation, achieved by using the Biot-Savart kernel, finally gives the fluctuating velocity field expressed as follows:

$$\mathbf{u}'(\mathbf{x}) = \sqrt{\frac{1}{N}} \sum_{k=1}^N \mathbf{K}_\sigma \left( \frac{\mathbf{x} - \mathbf{x}^k}{\sigma} \right) \times \alpha^k \quad (3)$$

where  $\alpha^k$  are random numbers which represent the eddies' intensities and  $\mathbf{K}_\sigma(\mathbf{y})$  is the Biot-Savart kernel, which is defined as  $\mathbf{K}_\sigma(\mathbf{y}) = \frac{q_\sigma(|\mathbf{y}|)}{|\mathbf{y}|^3} \mathbf{y}$  with  $q_\sigma(|\mathbf{y}|)$  a suitable shape function. It is important to remark here that the above Biot-Savart kernel comes from the solution of equation (2) with the assumption of a constant shape length scale  $\sigma$  and shape function  $q_\sigma$  in the  $x$ ,  $y$  and  $z$  directions.

**REYNOLDS STRESS TENSOR** One of the simplest functions chosen for the shape function  $q_\sigma$  is

$$q_\sigma\left(\frac{r^k}{\sigma}\right) = B[\sin(\pi \frac{r^k}{\sigma})]^2 \frac{r^k}{\sigma} \quad (4)$$

where  $r^k = \sqrt{(x-x^k)^2 + (y-y^k)^2 + (z-z^k)^2}$ ,  $\sigma$  is the eddy length scale and  $B$  is a scaling coefficient, here taken as  $B = \sqrt{\frac{15V_b}{16\pi\sigma^3}}$ .  $V_b$  is the volume of the box the eddy are convected through. In order to examine what the scheme returns for the Reynolds stresses, equation (3) can be manipulated and averaged, giving<sup>1</sup>

$$\begin{aligned} \langle u'u' \rangle &= \langle \alpha_2^2 \rangle \langle [q_\sigma(\frac{r^k}{\sigma})]^2 \frac{1}{\sigma^2} \frac{(z-z^k)^2}{(\frac{r^k}{\sigma})^6} \rangle \\ &+ \langle \alpha_3^2 \rangle \langle [q_\sigma(\frac{r^k}{\sigma})]^2 \frac{1}{\sigma^2} \frac{(y-y^k)^2}{(\frac{r^k}{\sigma})^6} \rangle \end{aligned} \quad (5)$$

Because of the symmetry of the eddy contributions in the  $y$  and  $z$  directions, and the scaling of  $q_\sigma$  noted above, the above

<sup>1</sup>Here only results for  $\langle u'u' \rangle$  are reported, though similar expressions are obtained for  $\langle v'v' \rangle$  and  $\langle w'w' \rangle$ .

expression can be simplified to give

$$\langle u'u' \rangle = \frac{\langle \alpha_3^2 \rangle}{2} + \frac{\langle \alpha_2^2 \rangle}{2} \quad (6)$$

To see how to scale the random numbers  $\alpha_j^k$  to give the desired stress anisotropy, it is convenient to work in the principal axes of the stress tensor, where  $\langle \alpha_1^k \rangle$ ,  $\langle \alpha_2^k \rangle$  and  $\langle \alpha_3^k \rangle$  can be related to the eigenvalues of the Reynolds stress in the principal axes ( $\lambda_1$ ,  $\lambda_2$  and  $\lambda_3$ ) by

$$\begin{aligned} \lambda_1 &= \frac{1}{2}(\langle \alpha_2^2 \rangle + \langle \alpha_3^2 \rangle) \\ \lambda_2 &= \frac{1}{2}(\langle \alpha_3^2 \rangle + \langle \alpha_1^2 \rangle) \\ \lambda_3 &= \frac{1}{2}(\langle \alpha_1^2 \rangle + \langle \alpha_2^2 \rangle) \end{aligned} \quad (7)$$

As a result, in order to reproduce the stress anisotropy,  $\alpha_i^k$  in equation (3) can be taken as

$$\alpha_i^k = (\sqrt{2(k' - \lambda_i)}) \varepsilon_i^k \quad (8)$$

where  $\varepsilon_i^k$  are random numbers having  $\langle \varepsilon_j^k \varepsilon_j^k \rangle = 1$ .

In order to obtain the stress field in the original reference frame, the  $\alpha^k$  must be transformed back from the principal axes frame to the global frame, using a rotational matrix as below:

$$(\alpha^k)^G = R_L^G (\alpha^k)^L \quad (9)$$

where the superscripts  $L$  and  $G$  refer respectively to the local and the global reference systems.

The final equation for the velocity fluctuations is then:

$$\mathbf{u}' = \sqrt{\frac{1}{N}} \sum_{k=1}^N \frac{q_\sigma(\frac{r^k}{\sigma})}{(\frac{r^k}{\sigma})^3} \frac{\mathbf{r}^k}{\sigma} \times [R_L^G (\sqrt{2(k' - \lambda_i)} \varepsilon_i^k)^L] \quad (10)$$

## TURBULENCE ANISOTROPY CLIPPING

As result of the square root in equation (8), the present method is not capable of reproducing every state of turbulence, since a very high anisotropy may lead to a negative argument of the square root. The limitation implied by equation (8) is that each normal stress must not be greater than the turbulent kinetic energy. To illustrate the restriction this places on the method, Figure 2 shows the Lumley triangle of possible turbulent stress anisotropy states, with the shaded region indicating the states for which equation (8) can be applied. The limitation might, from this, appear to be rather restrictive; comparing to the DNS data of [6] for a plane channel flow at  $Re_\tau = 395$ , the method above could only be applied to represent the stresses correctly for  $y^+ > 300$ .

A clipping methodology for the turbulence anisotropy is thus required, and in the present work this has been implemented by conserving the total turbulent kinetic energy required at the inlet, but redistributing the excess of energy in one direction into the other ones when one stress becomes too

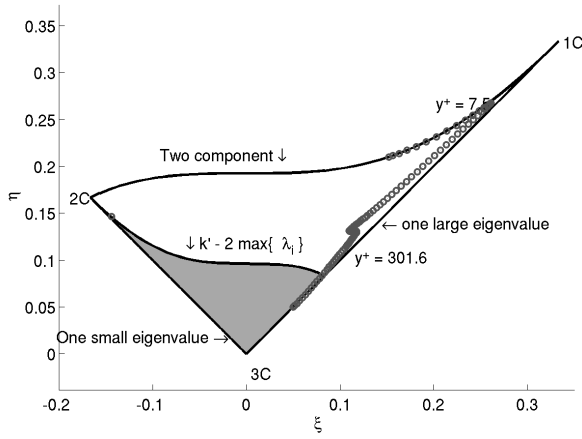


Figure 2. Lumley triangle for the DF-SEM. The axes are defined by:  $6\eta^2 = b_{ii}^2$ ;  $6\xi^3 = b_{ii}^3$  and  $b_{ij} = \frac{\langle u_i u_j \rangle}{\langle u_k u_k \rangle} - \frac{1}{3} \delta_{ij}$ , which is the non-isotropic part of the Reynolds stress tensor. The grey area refers to reproducible area:  $\sum_{i=1}^3 \lambda_i - 2 \max\{\lambda_1, \lambda_2, \lambda_3\} \geq 0$ . The circles represent the channel flow DNS at  $Re_\tau = 395$  of [6]. 1C, one-component; 2C, two-components.

large to apply equation (8). In practice, in the present channel flow case this means limiting  $\langle uu \rangle$ , and correspondingly increasing  $\langle vv \rangle$  and  $\langle ww \rangle$  near the wall. It should also be noted that since the clipping is applied to the stresses in principal axes, it also affects the shear stress, once the stresses are mapped back to the global reference frame.

Despite the above comments on Figure 2, the results to be presented below will show that although the stress anisotropy clipping is applied over a significant part of the channel inlet, its strongest influence is seen only in the near-wall region with  $y^+ < 75$  or so.

**MASS FLOW RATE CORRECTION** Separate from the above considerations of reproducing the Reynolds stresses, another problem was noted with the SEM and DF-SEM when applied to a wall-bounded case such as the present channel flow. It was noted the streamwise velocity fluctuations returned by equation (1) or (3) resulted in a non-constant bulk flow rate into the channel (although each eddy has zero mass flow, a numerical sampling of a finite number of them may return a non zero mass flow). This resulted in a time-dependent flow rate along the channel, giving rise to temporal variations in the pressure gradient along the channel as a result of non physical pressure fluctuations (as Figure 3 clearly highlights).

To avoid the above problem a bulk correction was applied to the inlet velocity profile by simply introducing a rescaling coefficient to ensure the total mass flow rate across the inlet plane remained constant. Numerical simulations showed this rescaling coefficient modified the velocity field by less than 1% in channel flows, and so its effect on the divergence free scheme was deemed negligible. When the massflow rescaling is applied the pressure fluctuations are highly decreased, as Fig. 4 sketches at  $y^+ = 395$ . The DF-SEM presents these numerical fluctuations only very close to the periodic condi-

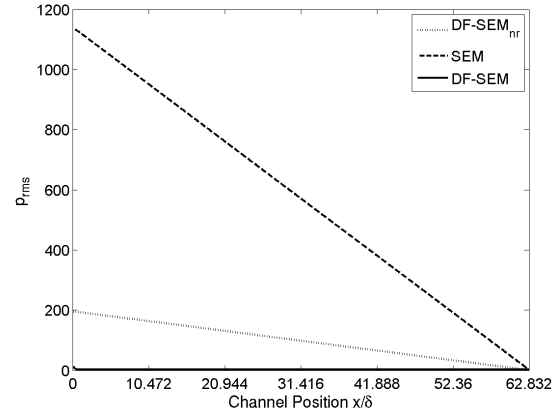


Figure 3. Pressure Fluctuation with non rescaled SEM and  $DF - SEM_{nr}$

tions, whilst at the center of the channel the affection is almost negligible. The SEM instead equally affect all the inlet location despite the mass flow reduction. On the other hand, it had a significant beneficial influence in reducing the overall computation time. Since the Code-Saturne solver employed in the present work uses a SIMPLER type of pressure-velocity coupling, the continually changing bulk pressure gradient along the channel resulted in a large number of iterations being required to solve the pressure correction equation. The above correction significantly reduced these, resulting in lower computational time requirements.

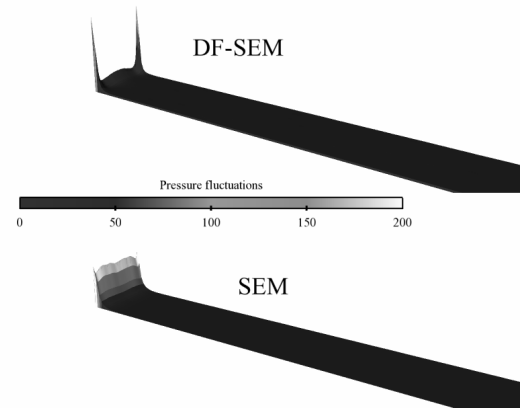


Figure 4. Pressure fluctuations at the inlet with the DF-SEM and the SEM ( $y^+ = 395$ )

## CHANNEL FLOW RESULTS

Channel flow simulations have been carried out to test the new method against some other commonly used ones. In the results presented below, DF-SEM refers to the divergence-free SEM method outlined above, whilst SEM refers to the original scheme of [4]. In both cases the bulk mass flow cor-

rection described above has been applied to the scheme. The third set of results correspond to simulations employing the VORTEX method of [2].

The simulations have been carried out for a channel flow with  $Re_\tau = 395$ . The sizes of the domain was  $20\pi \times 2 \times \pi$ , covered by a mesh of  $500 \times 46 \times 82$  cells, with  $y^+ \approx 1$  at the wall. The inlet conditions were generated by the three methods noted above, using DNS data for the turbulent stress levels.

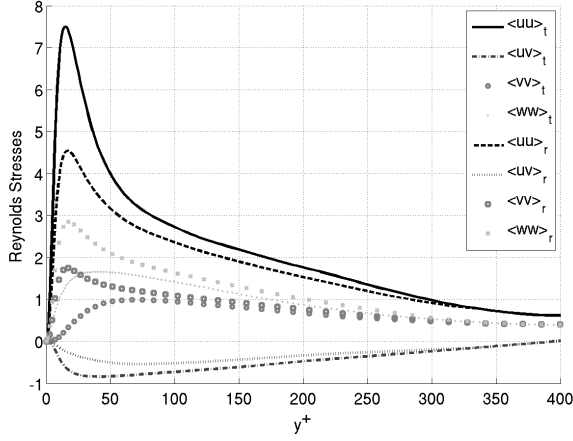


Figure 5. Reynolds stresses clipped by the DF-SEM. The superscripts t and r refers respectively to the DNS profiles and the clipped ones

Figure 5 shows the Reynolds stress profiles from DNS and those employed in the DF-SEM approach, clearly indicating the effect the clipping has on the inlet profiles from the DF-SEM. Exact stresses are reproduced only for  $y^+ > 300$ , although the clipping is relatively modest until  $y^+ > 75$ , where the DNS begins to show highly anisotropic turbulence.

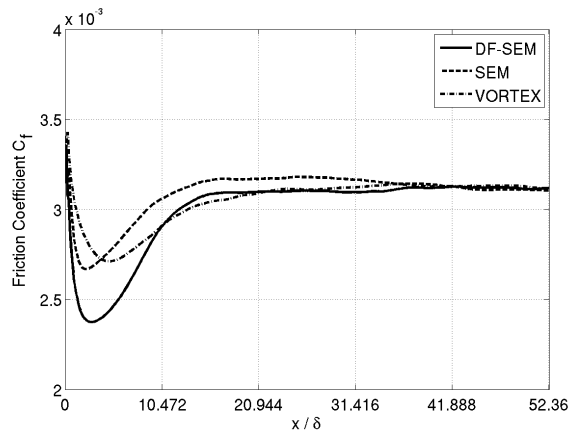


Figure 6. Friction coefficient development along the Channel - DNS inlet

**FRICTION COEFFICIENT** The developemnt of the friction coefficient along the channel is a convenient parameter to compare the performance of the three methods tested. The general behaviour, shared among all the simulations, and shown in Figure 7, is a sudden drop of  $C_f$ , followed by a recovery to the fully-developed value give by the LES scheme. Both the inital drop and the recovery rate are highly influenced by the synthetic turbulence used to define the inlet. The DF-SEM results in the largest initial drop among the tested methods but, on the other hand, has the shortest recovery length, whereas the SEM exhibits an overshoot of  $C_f$  before gradually returning to the final level. The VORTEX methodology shows the slowest recovery, even though its initial drop is the smallest among the methods tested.

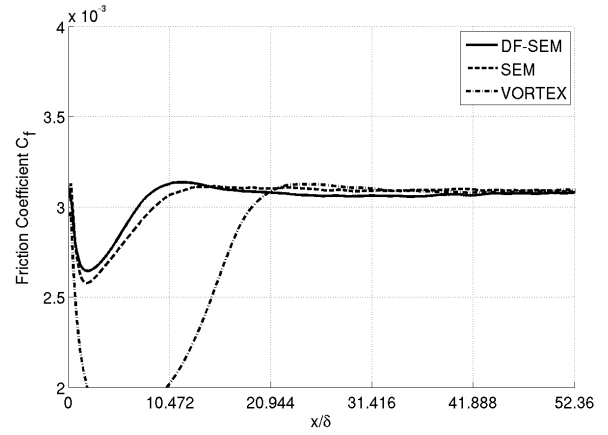


Figure 7. Friction coefficient development along the Channel - RANS inlet

In order to show more clearly the positive influence of the DF-SEM, a second channel flow has been performed, this time with inlet conditions coming from a previous RANS simulation (Eddy Viscosity Model,  $k - \omega$  SST). While the VORTEX method in this case decreases by far its performances, the DF-SEM substantially maintains the same developping length, as the SEM does. This is due to the fact that, because of the turbulence anisotropy clipping mentioned earlier, the DF-SEM is sensitive only to the turbulence level (kinetic energy) and not to the shear stress, which is always under-estimated.

**VELOCITY PROFILES** Figure 8 shows mean velocity profiles at a selection of streamwise locations from the simulation using the DF-SEM inlet conditions. There is a small underestimation of the velocity for  $y^+ < 40$  and  $x/\delta < 11$ , corresponding to the zone where the friction coefficient shows a dip towards the start of the channel. It should also be noted that it is in this near wall region where the clipping of the stress anisotropy has a significant effect on the Reynolds stresses employed in the DF-SEM.

**TURBULENT SHEAR STRESS** Profiles of the turbulent shear stress, shown in Figures 10, are particularly

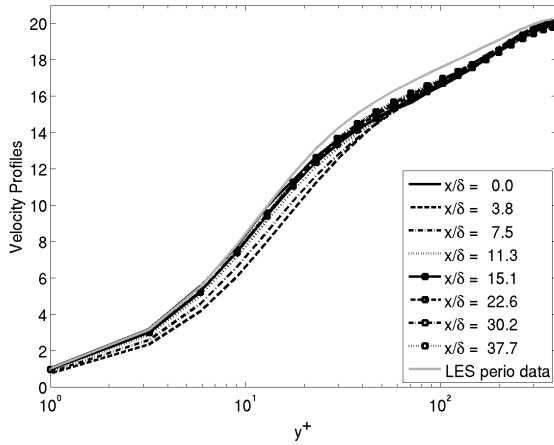


Figure 8. Velocity profiles - DF-SEM

interesting. Bearing in mind that the DF-SEM does not reproduce the precise state of turbulence for  $y^+ < 300$ , the inlet shear stress magnitude is always under estimated, as shown in Figure 9. However, for  $y^+ > 250$ ,  $\langle uv \rangle$  recovers almost instantaneously with the DF-SEM, and even over the rest of the channel the profiles beyond  $x/\delta \approx 10$  are very close to the fully developed LES data.

The SEM, on the other hand, exhibits a rather long recovery, and the overshoot noticed in the friction coefficient can also clearly be seen in the  $\langle uv \rangle$  profiles. The VORTEX method has a very peculiar behaviour: a very low inlet shear stress is provided by the method itself, consistent with the fact that the method applies the fluctuations in  $x$  direction using a separate equation (so  $u$  and  $v$  are not correlated). At the first downstream cell ( $x/\delta = 0$ ) only for  $y^+ < 20$  is there any agreement with the fully developed values. Nevertheless, the method is able to recover rapidly from this initial underestimation and at  $x/\delta = 3.8$  the prediction of the shear stress is consistent with the periodic solution for  $y^+ > 200$  as well. The remaining region,  $20 < y^+ < 200$  develops over a longer distance, leading to the lengthy recovery of  $C_f$  noted earlier.

**TURBULENT KINETIC ENERGY** Figures 9 show profiles of the turbulent kinetic energy along the channel using the three different inlet treatments. The VORTEX methodology introduces low inlet turbulence levels, as shown in Figure 9. For both the DF-SEM and the SEM it seems that part of the energy is dissipated at the beginning of the channel (since the profile at the inlet would give a peak corresponding roughly to the LES peak), and then is recovered as the flow develops along the channel. In all three cases the energy profiles reach their fully-developed values at approximately  $x/\delta = 10$  and again, as already noticed, the SEM exhibits a kind of overshoot which affects its performance.

**FOURIER ANALYSIS** To shed further light on the comparison between the different inlet generation methods, a Fourier analysis of the inlet velocity signal has been per-

formed. The selected locations where the spectral analysis has been performed are near the centreline, at  $y^+ = 390$  and closer to the wall at  $y^+ = 39.5$ , shown in Figure 11.

Each case is compared to the spectra obtained from a fully-developed LES channel flow calculation. The figures show a significant underprediction of the fluctuations in the VORTEX method at  $y^+ = 390$ . The SEM shows a strange behaviour at high frequency, where a double peak is present. This may be due to the length scale and eddy convection velocity definition. The DF-SEM produces fluctuations with higher frequency than the SEM. This is mainly due to the use of the same length scales as in the SEM even though the DF-SEM eddies produce a different velocity distribution around the eddy, and in particular a double lobes (see Fig. [insert picture of the eddy velocity distribution]).

## CONCLUSIONS

The new method defined here, based on the existing SEM suggested by [4], let the user generate a divergence free synthetic turbulence velocity field. This feature, not noticed in any other synthetic turbulence algorithm, helps reduce the region affected by the method itself. Channel flow results demonstrated that the friction coefficient decreases the zone where it develops to a periodic value. Regarding the shear stress instead, the new method performs very well at  $y^+ > 250$ , because of its own nature and a lack in reproducing very high anisotropic turbulent structures.

## REFERENCES

- [1] N. Jarrin, R. Prosser, J. Uribe, S. Benhamadouche, and D. Laurence, "Reconstruction of turbulent fluctuations for hybrid RANS/LES simulations using a Synthetic-Eddy method," *International Journal of Heat and Fluid Flow*, vol. 30, pp. 435–442, June 2009.
- [2] M. E. Sergent, *Vers une Methodologie de Couplage Entre la Simulation des Grande Echelles et les Modeles Statistiques*. PhD thesis, Ecole Central de Lyon, 2002.
- [3] M. Pamiès, P.-É. Weiss, E. Garnier, S. Deck, and P. Sagaut, "Generation of synthetic turbulent inflow data for large eddy simulation of spatially evolving wall-bounded flows," *Physics of Fluids*, vol. 21, no. 4, p. 045103, 2009.
- [4] N. Jarrin, S. Benhamadouche, D. Laurence, and R. Prosser, "A synthetic-eddy-method for generating inflow conditions for large-eddy simulations," *International Journal of Heat and Fluid Flow*, vol. 27, pp. 585–593, Aug. 2006.
- [5] T. S. Lund, X. Wu, and K. D. Squires, "Generation of turbulent inflow data for Spatially-Developing boundary layer simulations," *Journal of Computational Physics*, vol. 140, pp. 233–258, Mar. 1998.
- [6] R. D. Moser, J. Kim, and N. N. Mansour, "Direct numerical simulation of turbulent channel flow up to  $Re_{\tau} = 590$ ," *Physics of Fluids*, vol. 11, no. 4, pp. 943–945, 1999.

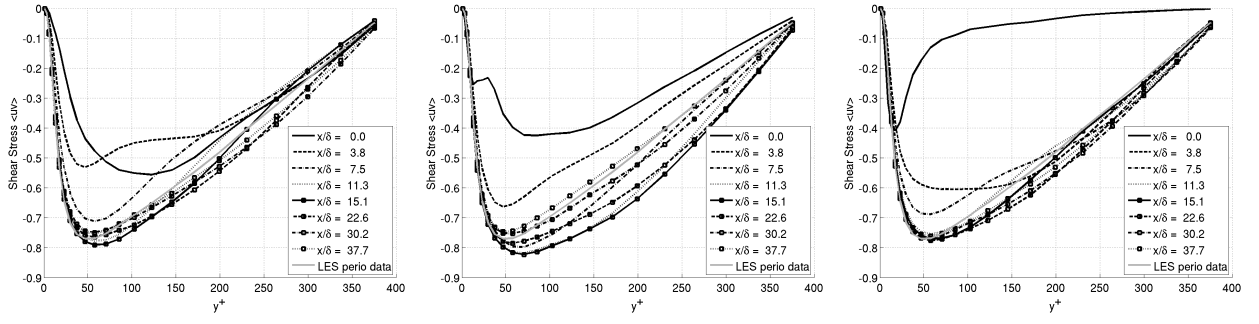


Figure 9. Shear stress profiles - DF-SEM / SEM / VORTEX

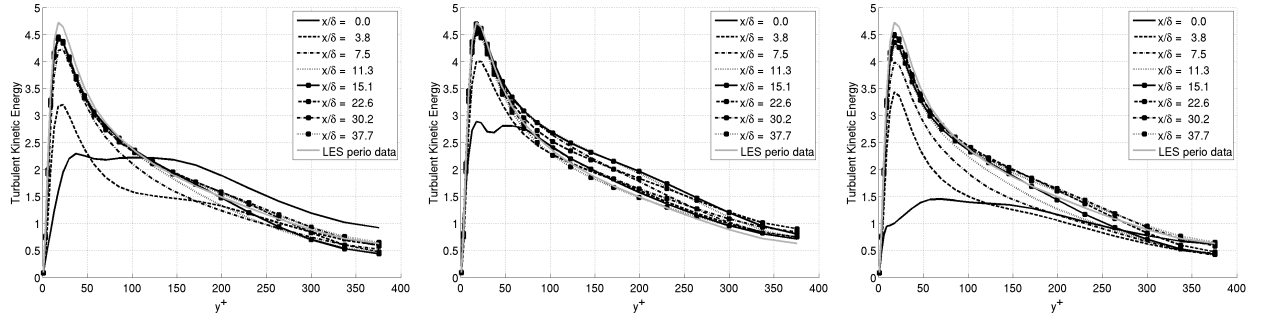


Figure 10. Turbulent Kinetic Energy profiles - DF-SEM / SEM / VORTEX

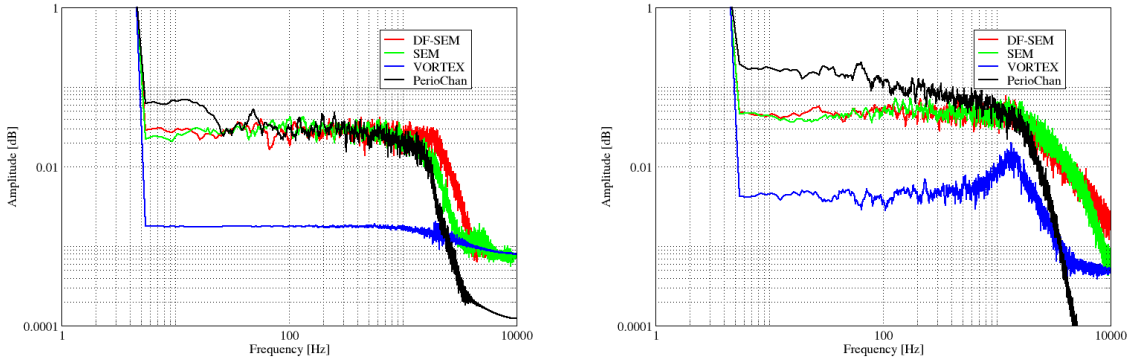


Figure 11. Fourier analysis of U at  $y^+ = 390$  and  $y^+ = 39.5$